scientific reports

Check for updates

OPEN

Numerical study of non-Darcy hybrid nanofluid flow with the effect of heat source and hall current over a slender extending sheet

Zehba Raizah[1], Hussam Alrabaiah[2,3], Muhammad Bilal[4], Prem Junsawang[5]✉ & Ahmed M. Galal[6,7]

The current evaluation described the flow features of Darcy Forchhemier hybrid nanoliquid across a slender permeable stretching surface. The consequences of magnetic fields, second order exothermic reaction, Hall current and heat absorption and generation are all accounted to the fluid flow. In the working fluid, silicon dioxide (SiO_2) and titanium dioxide (TiO_2) nano particulates are dispersed to prepare the hybrid nanoliquid. TiO_2 and SiO_2 NPs are used for around 100 years in a vast number of diverse products. The modeled has been designed as a nonlinear set of PDEs, Which are degraded to the dimensionless system of ODEs by using the similarity transformation. The reduced set of nonlinear ODEs has been numerically estimated through bvp4c package. The outcomes are tested for validity and consistency purpose with the published report and the ND solve technique. It has been noted that the energy curve lessens with the influence of thermodiffusion, Brownian motion and rising number of nanoparticles, while boosts with the result of magnetic field. Furthermore, the concentration outline of hybrid nanoliquid improves with the upshot of chemical reaction.

Abbreviations

n	Power index
U_0	Reference velocity
m	Hall current
K^*	Permeability factor
2D	Two-dimension
F	Non-uniform inertia factor
T	Temperature
Nt	Thermodiffusion
Pr	Prandtl number
μ_{hnf}	Viscosity
$(\rho C_p)_{hnf}$	Thermal capacity
k_{hnf}	Thermal conductivity
$\phi_1 = \phi_{SiO_2}$	Nanoparticles volume friction
$C_2H_6O_2$	Ethyne glycol
(u, v, w)	Velocity component
A	Stretching constant
U_w	Stretching velocity

[1]Department of Mathematics, College of Science, King Khalid University, Abha, Saudi Arabia. [2]College of Engineering, Al Ain University, Al Ain, United Arab Emirates. [3]Mathematics Department, Tafila Technical University, Tafila, Jordan. [4]Department of Mathematics, City University of Science and IT, Peshawar 25000, Pakistan. [5]Department of Statistics, Faculty of Science, Khon Kaen University, Khon Kaen 40002, Thailand. [6]Department of Mechanical Engineering, College of Engineering in Wadi Alddawasir, Prince Sattam Bin Abdulaziz University, Wadi Alddawasir, Saudi Arabia. [7]Production Engineering and Mechanical Design Department, Faculty of Engineering, Mansoura University, Mansoura 35516, Egypt. ✉email: prem@kku.ac.th

Kc^2	Chemical reaction rate
Q_0	Heat source
MHD	Magnetohydrodynamics
C	Concentration
λ	Porosity factor
Nb	Brownian motion
Gr	Grashof number
ρ_{hnf}	Density
$(\rho\beta_T)_{hnf}$	Thermal expansion
σ_{hnf}	Electrical conductivity
$\phi_2 = \phi_{TiO_2}$	Nanoparticles volume friction
TiO_2	Titanium dioxide
SiO_2	Silicon dioxide

The analysis of fluid flow over a slendering surface has frequent implementations in various fields, containing manufacture of glass, aerodynamic, polymer industry, firmness of plastic slips and metal tubular[1–3]. Gul et al.[4] examined and evaluated the proficiency of a hybrid nanofluid along an increasing sheet. It was discovered that the magnetism influence altered the instability of liquid. Bilal et al.[5] employed the PCM methodology to imitate the movement of nanoliquids through a stretchable material with the effects of suction and injection. The physical and chemical properties of nanofluid flow passing through permeable stretching was documented by Safwa et al.[6]. Moreover, Hussain et al.[7] reported the energy conversions of MHD nanoliquid flow along an elongating surface. Shuaib et al.[8] described the ferrofluid flow along with the characteristics of energy conveyance through spinning sheet. Hussain et al.[9] assessed the energy transport through nanoliquid flow over an extending cylinder. Uddin et al.[10] analysed the energy transmission through water-based nanoliquid across an expanding surface. Rasool et al.[11] documented the nanoliquid flow across a contracting surface. Ahmad et al.[12] assessed nanoliquid fluid across a slender stretching sheet.

Hybrid nanofluid has greater thermal efficiency and mostly utilized in industry for cooling purposes[13]. Hybrid nanofluid work in solar energy, energy transition, air conditioners, generators, the vehicle sector, radioactive systems, electrical coolers, ships, biotechnology and transmitters[14–16]. TiO_2 and SiO_2 have non-toxic, non-reactive characteristics and absorb UV rays used for skin cancer, drug delivery, recording devices and solar cells[17]. Traciak et al.[18] conducted an experimentally assessed the density, optical characteristics and surface tension of SiO_2-containing nanoliquids based on ethylene glycol. Using the bvp4c software, Bhatti et al.[19] provided a detailed discussion of SiO2 and carbon nanocrystals over an elastic substrate. Ahmed et al.[20] scrutinized the nanoliquid flow and energy conveyance through Al_2O_3 and TiO_2 nps based nanoliquid, to augments the thermal efficiency of base solvent, such as thermal diffusivity and heat transport coefficient. Khashi'ie et al.[21,22] highlighted the comportment of Al_2O_3-Cu based hybrid nanoliquid flow and its thermal properties as they were driven by an elongating Riga plate. Alwawi et al.[23] addressed the impact of magnetism on nanofluid streaming in the scenario of coupled convection across a circular cylinder. The findings show that increasing the coupled convection factor's value improves the Nusselt number, velocity, skin friction and rotational velocity while reducing the thermal contour's trends. Abbasi et al.[24] comparatively reported the thermal assessment of three distinct sorts of nano particulates, including TiO_2, SiO_2 and aluminum oxide through curved sheet. Khashi'ie et al.[25] used Cu-Al_2O_3 hybrid nanoparticles to study the Blasius flow across a rotating plate. De[26] and Mondal et al.[27] investigated the combined influence of Soret-Dufour interactions in a nanoliquid flow. Recently, a number of investigators have described on the evaluation of hybrid nanoliquid flow over distinct configuration[28–32].

Hall current can be detected if the fluid density is small, or the magnetic flux amplitude is strong. In many practical operations that call for an intense electric affect and smaller atomic concentration, hall effects should not be undervalued. Electron transport, where electrons move more quickly than ions, is what results in isotropic conductivity. Ohm's law needs to be revised for the purposes to consider the Hall effect. It has several applications in Hall activators, circuits, pumps, electric inverters, turbines and other equipment, Nanoliquid flow with the upshot of Hall current and magnetic effect has drawn the attention of scientists[33,34]. Using an extended sheet, Khan and Nadeem[35] examined a spinning Maxwell nanoliquid flow with a magnetism, Hall current and kinetic energy. An asymmetrical reactive nanoliquid flow induced by a magnetization revolving plate and the Hall impact is described by Acharya et al.[36] along with the flow dynamics and energy variations. They found that the energy transference was improved by 84.61% by nanocomposites. The Hall effect in nanofluid flow has recently been the subject of numerous investigations[37–40].

The purpose of the current assessment is to study the flow features of Darcy Forchhemier hybrid nanoliquid across a slender permeable stretching surface. The consequences of magnetic fields, second order exothermic reaction, Hall current and heat absorption and generation are all accounted to the fluid flow. In the working fluid, SiO_2 and TiO_2 nano particulates are dispersed to prepare the hybrid nanoliquid. The modeled has been designed as a nonlinear set of PDEs. Which are transmute to the dimensionless system of ODEs by using the similarity replacement. The reduced set of nonlinear ODEs has been numerically estimated through bvp4c package.

Mathematical framework

We assumed a steady 2D MHD hybrid nanoliquid flow through impermeable slendering substrate. The surface is stretching with velocity $U_w(x) = (x+b)^n U_0$, as described in Fig. 1, where n is the power index. The sheet irregularity is assumed as $y = A(x+b)^{\frac{1-n}{2}}$, ($A$ is the stretching constant). The Hall and magnetic effect are

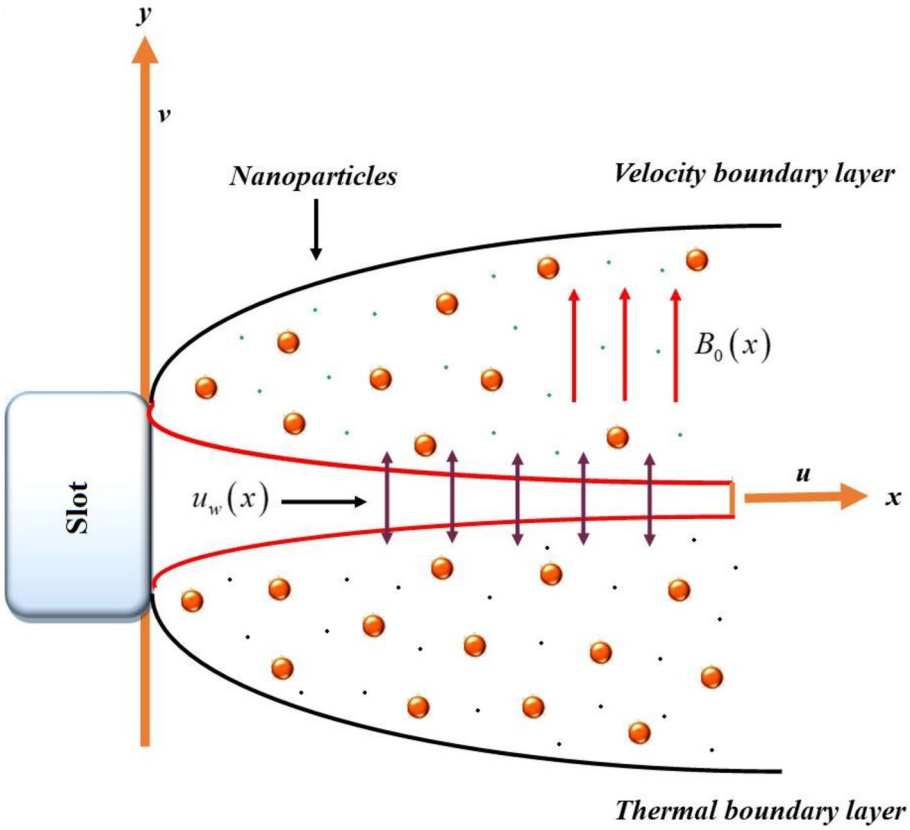

Figure 1. The fluid flow across a slandering expanding cylinder.

employed for flow motion in y-direction. Heat source, Brownian motion, thermo-diffusion and chemical reactions are all observed in current analysis.

The basic equations responsible for the fluid flow are characterized as[41]:

$$\frac{\partial u}{\partial x}+\frac{\partial v}{\partial y}=0, \tag{1}$$

$$\rho_{hnf}\left(u\frac{\partial u}{\partial x}+v\frac{\partial u}{\partial y}\right)=\mu_{hnf}\frac{\partial^2 u}{\partial y^2}-\frac{\sigma_{hnf}}{1+m^2}B^2(x)(u+mw)-\frac{\upsilon_{hnf}}{K^*}u-\frac{1}{\rho_{hnf}}Fu^2, \tag{2}$$

$$\rho_{hnf}\left(u\frac{\partial w}{\partial x}+v\frac{\partial w}{\partial y}\right)=\mu_{hnf}\frac{\partial^2 w}{\partial y^2}-\frac{\sigma_{hnf}}{1+m^2}B^2(x)(mu-w)-\frac{\upsilon_{hnf}}{K^*}w-\frac{1}{\rho_{hnf}}Fw^2, \tag{3}$$

$$\left(u\frac{\partial T}{\partial x}+v\frac{\partial T}{\partial y}\right)=\frac{k_{hnf}}{(\rho C_p)_{hnf}}\left(\frac{\partial^2 T}{\partial y^2}\right)+\left(D_B\frac{\partial T}{\partial y}\frac{\partial C}{\partial y}+\frac{D_T}{T_\infty}\left(\frac{\partial T}{\partial y}\right)^2\right)+\frac{Q_0(T-T_\infty)}{\rho C_p}, \tag{4}$$

$$\left(u\frac{\partial C}{\partial x}+v\frac{\partial C}{\partial y}\right)=D_B\left(\frac{\partial^2 C}{\partial y^2}\right)+\frac{D_T}{T_\infty}\frac{\partial^2 T}{\partial y^2}-Kc^2(C-C_\infty), \tag{5}$$

here, $m=\tau_e w_e$ is the Hall current, Kc^2, Q_0, K^* and $F=C_b/rK^{*1/2}$ are the chemical reaction rate, heat source, permeability factor and non-uniform inertia factor respectively.

The initial and boundary conditions are:

$$\left.\begin{aligned} &u=U_w(x)=U_0(x+b)^n,\ v=0,\ w=0,\ D_B\frac{\partial C}{\partial y}+\frac{D_T}{T_\infty}\frac{\partial T}{\partial y}=0,\ T=T_w \text{ at } y=A(x+b)^{\frac{1-n}{2}}\\ &u\to 0,\ T\to T_\infty,\ w\to 0,\ C\to C_\infty \text{ as } y\to\infty. \end{aligned}\right\} \tag{6}$$

The transformation variables are:

$$\eta = y\sqrt{\frac{n+1}{2}\frac{U_0}{\nu_f}(x+b)^{m-1}},\ \psi = \sqrt{\frac{2}{n+1}\nu_f U_0 (x+b)^{m+1}}\, f(\eta),\ \varphi(\eta) = \frac{C-C_\infty}{C_w - C_\infty},$$
$$w = U_0(x+b)^n h(\eta),\ \theta(\eta) = \frac{T-T_\infty}{T_w - T_\infty}. \tag{7}$$

By merging Eq. (7) in Eqs. (1)–(6), we get:

$$f''' + \frac{\vartheta_1}{\vartheta_2}\left(\left(ff'' - \frac{2n}{n+1}Frf'^2\right) - \frac{\vartheta_3}{\vartheta_1}\left(\frac{2M}{(n+1)(1+m^2)}\right)f' + \lambda mg\right) = 0, \tag{8}$$

$$g'' + \frac{\vartheta_1}{\vartheta_2}\left(\left(fg' - \frac{2n}{n+1}Frgf'\right) - \frac{\vartheta_3}{\vartheta_1}\left(\frac{2M}{(n+1)(1+m^2)}\right)mf' - \lambda g\right) = 0, \tag{9}$$

$$\theta'' + Pr\frac{\vartheta_4}{\vartheta_5}\left(f\theta' + Nb\,\varphi'\theta' + Nt\,\theta'^2\right) + Q_1\theta = 0, \tag{10}$$

$$\varphi'' + \frac{Nt}{Nb}\theta'' + Lef\varphi' - Kr\varphi = 0. \tag{11}$$

here, $\vartheta_1 = \frac{\rho_{hnf}}{\rho_f}$, $\vartheta_2 = \frac{\mu_{hnf}}{\mu_f}$, $\vartheta_3 = \frac{\sigma_{hnf}}{\sigma_f}$, $\vartheta_4 = \frac{(\rho C_p)_{hnf}}{(\rho C_p)_f}$, $\vartheta_5 = \frac{k_{hnf}}{k_f}$.

The conditions for system of ODEs are:

$$\left.\begin{aligned} &f(\eta) = \eta\left(\frac{1-n}{1+n}\right),\ Nb\,\varphi'(\eta) + Nt\,\theta'(\eta) = 0,\ f'(\eta) = 1,\ g(\eta) = 0,\ \theta(\eta) = 1 \\ &f' \to 0,\ g \to 0,\ \theta \to 0,\ \varphi \to 0\ as\ \eta \to \infty \end{aligned}\right\} \tag{12}$$

here, the M, λ, Pr, Nt, Nb, Fr, Q_1, Le, Gr, δ,, Gc and Kr is mathematically expressed as:

$$M = \frac{B_0^2\sigma_f}{\rho_f T_\infty},\ Pr = \frac{\mu_f(\rho C_p)_f}{\rho_f k_f},\ \lambda = \frac{\nu}{k^* b},\ Nt = \frac{\tau D_T(T_w - T_\infty)}{\nu_f T_\infty},\ Fr = \frac{C_b}{K^{*1/2}},\ Nb = \frac{\tau D_B C_\infty}{\nu_f},\ Q_1 = \frac{xQ_0}{\rho C_p},$$
$$Le = \frac{\nu_f}{D_B},\ \delta = A\sqrt{\frac{n+1}{2}\frac{U_0}{\nu_f}},\ Gr = \frac{g\beta_{T_f}(T_w - T_\infty)n}{U_w^2},\ Gc = \frac{g\beta_{C_f}(C_w - C_\infty)n}{U_w^2},\ Kr = \frac{Kc^2}{b}. \tag{13}$$

The physical interest quantities are:

$$C_{f_x} = \frac{2\tau_{w_1}}{U_w^2\rho_f},\ C_{f_z} = \frac{\tau_{w_2}}{U_w^2\rho_f},\ Nu = \frac{q_w\,(x+b)}{(T_w - T_\infty)k_f},\ Sh = \frac{j_w\,(x+b)}{(C_w - C_\infty)D_B}. \tag{14}$$

where,

$$\left.\begin{aligned} &\tau_{w_1} = \mu_{hnf}\left(\frac{\partial u}{\partial y}\right)_{y=A(x+b)^{\frac{1-n}{2}}},\ \tau_{w_2} = \mu_{hnf}\left(\frac{\partial v}{\partial y}\right)_{y=A(x+b)^{\frac{1-n}{2}}}, \\ &q_w = -k_{hnf}\left(\frac{\partial T}{\partial y}\right)_{y=A(x+b)^{\frac{1-n}{2}}},\ j_w = -D_B\left(\frac{\partial C}{\partial z}\right)_{y=A(x+b)^{\frac{1-n}{2}}}. \end{aligned}\right\} \tag{15}$$

The dimensionless structure of Eq. (14) is:

$$\left.\begin{aligned} &C_{fr_x} = \sqrt{Re_x}C_{fx} = (1-\phi_1)^{-2.5}(1-\phi_2)^{-2.5}\sqrt{2(n+1)}\,f''(0), \\ &C_{fr_z} = \sqrt{Re_x}C_{fz} = (1-\phi_1)^{-2.5}(1-\phi_2)^{-2.5}\sqrt{2(n+1)}\,g'(0), \\ &Nu_r = \frac{Nu}{\sqrt{Re_x}} = -\frac{k_{hnf}}{k_f}\sqrt{\frac{n+1}{2}}\theta'(0),\ Sh_r = \frac{Sh}{\sqrt{Re_x}} = -\sqrt{\frac{n+1}{2}}\varphi'(0). \end{aligned}\right\} \tag{16}$$

Numerical methodology

The system of Eqs. (8)–(12) are simplified to 1st order set of ODEs and solved through bvp4c package as[42,43]

$$\left.\begin{aligned} &\xi_1 = f(\eta),\ \xi_3 = f''(\eta),\ \xi_5 = g'(\eta),\ \xi_7 = \theta'(\eta),\ \xi_9 = \varphi'(\eta), \\ &\xi_2 = f'(\eta),\ \xi_4 = g(\eta),\ \xi_6(\eta) = \theta(\eta),\ \xi_8 = \varphi(\eta). \end{aligned}\right\} \tag{17}$$

By putting (17) in (8–12), we get:

$$\xi_3' + \frac{\vartheta_1}{\vartheta_2}\left(\left(\xi_1\xi_3 - \frac{2n}{n+1}Fr\xi_2^2\right) - \frac{\vartheta_3}{\vartheta_1}\left(\frac{2M}{(n+1)(1+m^2)}\right)\xi_2 + \lambda m\xi_4\right) = 0, \tag{18}$$

$$\xi_5' + \frac{\vartheta_1}{\vartheta_2}\left(\left(\xi_1\xi_5 - \frac{2n}{n+1}Fr\xi_4\xi_2\right) - \frac{\vartheta_3}{\vartheta_1}\left(\frac{2M}{(n+1)(1+m^2)}\right)m\xi_2 - \lambda\xi_4\right) = 0, \tag{19}$$

$$\xi_7 + Pr\,\frac{\vartheta_4}{\vartheta_5}\left(\xi_1\xi_7 + Nb\,\xi_9\xi_7 + Nt\,\xi_7^2\right) + Q_1\xi_6 = 0, \tag{20}$$

$$\xi_9' + \frac{Nt}{Nb}\xi_7' + Le\xi_1\xi_9 - Kr^2\xi_8 = 0. \tag{21}$$

the transform conditions are:

$$\left.\begin{aligned} &\xi_1(\eta) = \eta\left(\frac{1-n}{1+n}\right),\ Nb\,\xi_9(\eta) + Nt\,\xi_7(\eta) = 0,\ \xi_2(\eta) = 1,\ \xi_4(\eta) = 0,\ \xi_6 = 1 \\ &\xi_2 \to 0,\ \xi_4 \to 0,\ \xi_6 \to 0,\ \xi_8 \to 0\ as\ \eta \to \infty \end{aligned}\right\} \tag{22}$$

Result and discussion

This segment estimates the exhibition of velocity, energy and concentration outlines versus interest constraints and explain the physics behind each table and figures. The dimensionless set of ODEs (Eqs. (18)–(22)) are solved through bvp4c package.

Velocity curve $f'(\eta)$. Figure 2a–d communicates the demonstration of velocity $f'(\eta)$ curve versus m, δ, n, ϕ_1, ϕ_1, Gc and Gr respectively. Figure 2a,b revealed that flow velocity amplifies with the outcome of m and diminishes with the impact of δ. Figure 2c,d exhibits that flow velocity augments with the influence of n and lessen with the impact of ϕ_1, ϕ_2 respectively. The result of n decreases the shear stress of surface, as a result the fluid velocity improves with action of n. The developing amount of $TiO_2 + SiO_2$ nps grows the fluid viscosity, which triggers the retardation effect. Figure 2e,f emphasized that velocity outline boosts with the increment of thermal and mass Grashop number. The extending velocity of surface drops with the upshot of Gc and Gr which triggers the rises in the velocity outline.

Figure 3a–d demonstrated the comportment of $g(\eta)$ outline verssu parameter m, n, δ, Fr and M. Figure 3a–b revealed that the flow velocity considerably upsurges with the change of m and n. While declines with the addition of δ and M. The magnetic upshot causes Lorentz effect, which prevents the flow moment, so the velocity profile drops. Figure 3e presents that the consequences of Fr pointedly de accelerates the velocity field in the radial direction.

Energy curve $\theta(\eta)$. Figure 4a–d demonstrates the arrangement of temperature $\theta(\eta)$ curve against δ, m, n and Q. Figure 4a,b describes that the energy $\theta(\eta)$ outline enlarged with the action of m and reduces under the upshot of δ. Hall current result also creates confrontation, which uplifts the energy contour as perceived in Fig. 4a. Figure 4c,d represent the significances of n and Q, that their effects augment the energy profile of $SiO_{42} + TiO_2/C_2H_6O_2$–$H_2O$ hybrid nanoliquid. The consequence of Q term operational as a energy mediator for the nanoliquid, which directly effects the temperature outline $\theta(\eta)$.

Figure 5a–d emphasized the appearance of heat $\theta(\eta)$ contour relative to Nb, Nt, ϕ_1, ϕ_1 and M. Figure 5a–c designated that fluid energy curve drops with the effect of Nb, Nt and ϕ_1, ϕ_1, while enhances with the influence of magnetic field. The mounting number of nano particulates intensifies the flow velocity as well as the heat capacity of the ordinary fluid, which fallouts such scenario. As earlier deliberated that the repellant strength created by the magnetic field, absolutely effects the energy curve $\theta(\eta)$.

Mass profile $\varphi(\eta)$. Figure 6a–c defined the exhibition of concentration $\varphi(\eta)$ contur versus m, δ, n and Kr. The concentration conversion of hybrid nanoliquid intensify with the upshot of m and declines with the impact of δ as exhibited in Fig. 6a,b. Figure 6c,d described that the upshot of Kr and n both augments the mass transport. The factor Kr boosts the kinetic force within the nanofluid, which results in the quick communication of concentration $\varphi(\eta)$.

Figure 7 emphasized the relative examination of nanofluid ($SiO_2 + TiO_2$) and hybrid nanoliquid ($SiO_2 + TiO_2/C_2H_6O_2$–H_2O) for the energy and the velocity outline. Tables 1 and 2 represent the tentative values and mathematical model for SiO_2, TiO_2 and base fluid. Table 3 described the numerical calculation of the present outcomes with the ND solver approach, to approve the authenticity of the results. Table 4 discovered the arithmetic valuations of $SiO_2 + TiO_2/C_2H_6O_2$–H_2O hybrid nanoliquid for C_{f_x}, C_{f_z}, Nu_r and Sh_r. It is identified that the upshot of m augments the energy interaction rate and drag force.

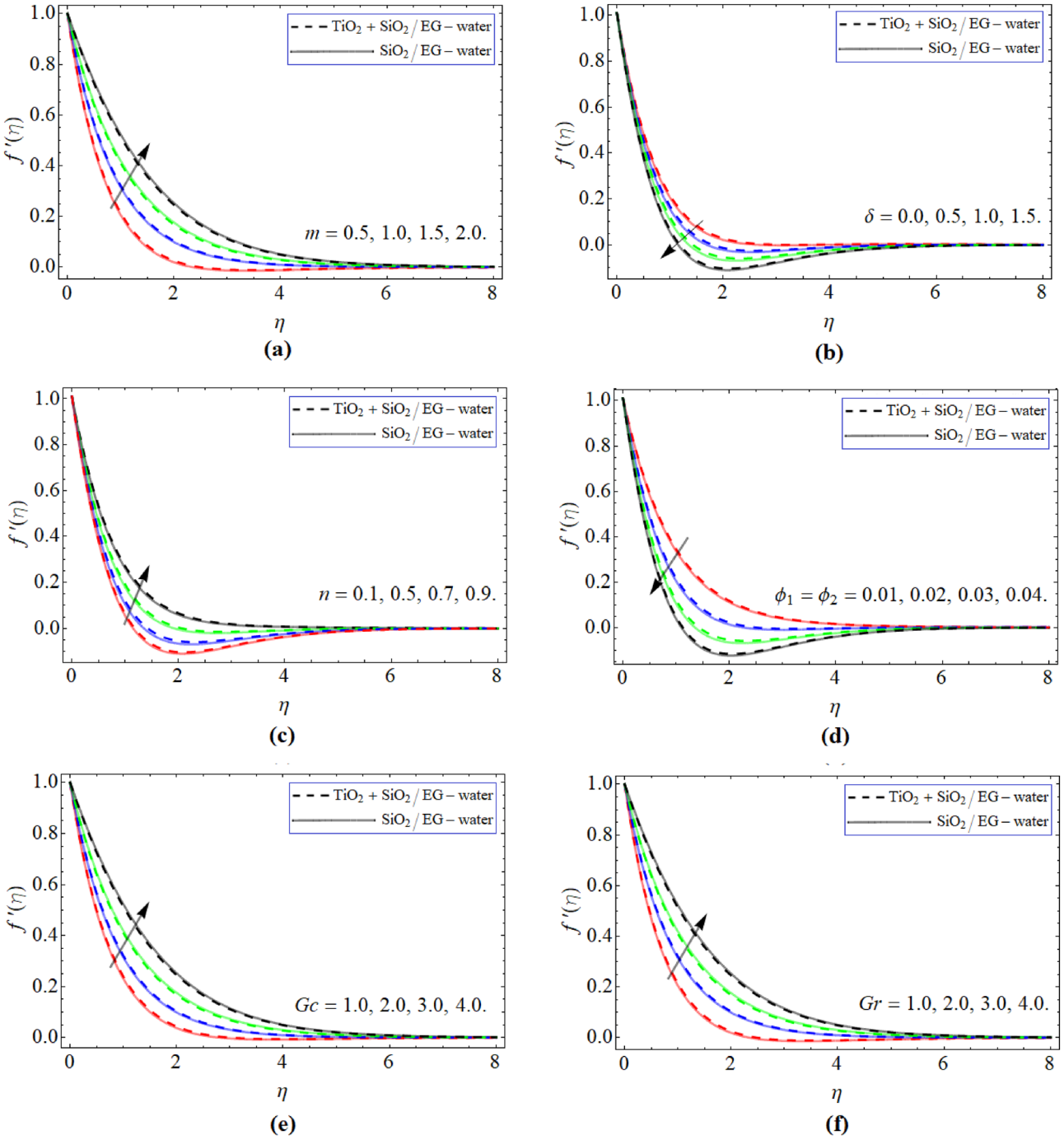

Figure 2. The exposition of velocity $f'(\eta)$ curve versus constraints $m, \delta, n, \phi_1, \phi_2$, Gc and Gr respectively.

Conclusion

We have examined the flow features of hybrid nanoliquid through a slender stretching surface. The consequences of second order exothermic reaction, heat source, Hall current and magnetic fields are all also described. The modeled equations are assessed by using the numerical approach bvp4c package. The important conclusions are:

- The $f'(\eta)$ outline augments with the outcome of n and m and while reduces with the rising quanitity of nano particulates ϕ_1, ϕ_2 and parameter δ.
- The velocity $g(\eta)$ curve substantially upsurges with effect of n and m. While decresaes with the effect of δ and M.

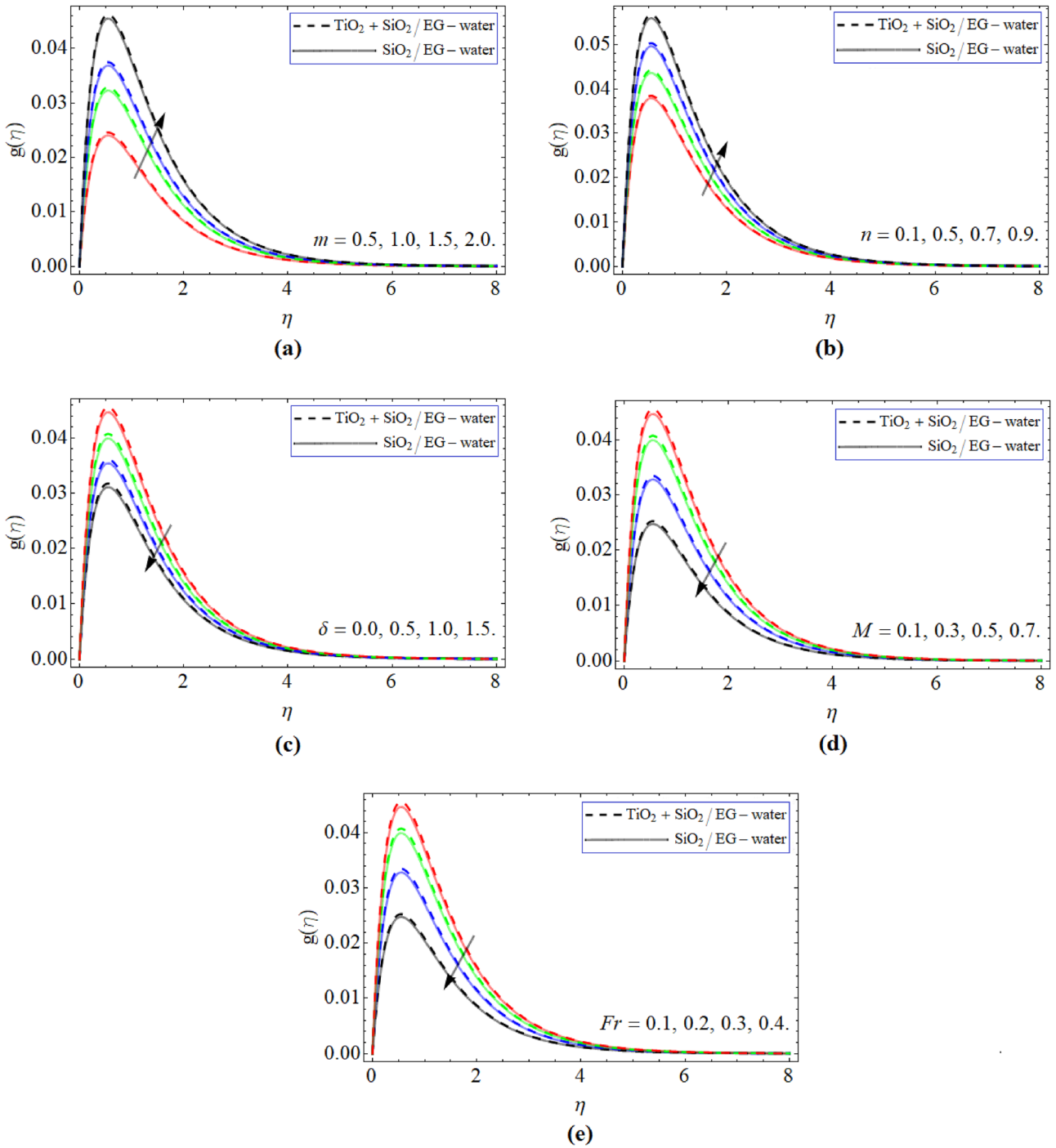

Figure 3. The exposition of velocity $g(\eta)$ curve versus the m, n, M, δ and Fr respectively.

- The energy $\theta(\eta)$ curve is enhances with the variation of m and diminishes with the δ.
- The energy $\theta(\eta)$ contour diminish with the influence of Nb, Nt and ϕ_1, ϕ_1, while boosts with the outcome of magnetic effect.
- The concentration $\varphi(\eta)$ outline of hybrid nanoliquid improves with the upshot of Kr and n.
- The current model may be expanded to other type of fluid and can be used different chemical composition nanoparticles in the base fluid for desire output. Furthermore, different numerical, analytical and fractional methods can also be used to solve such problems.

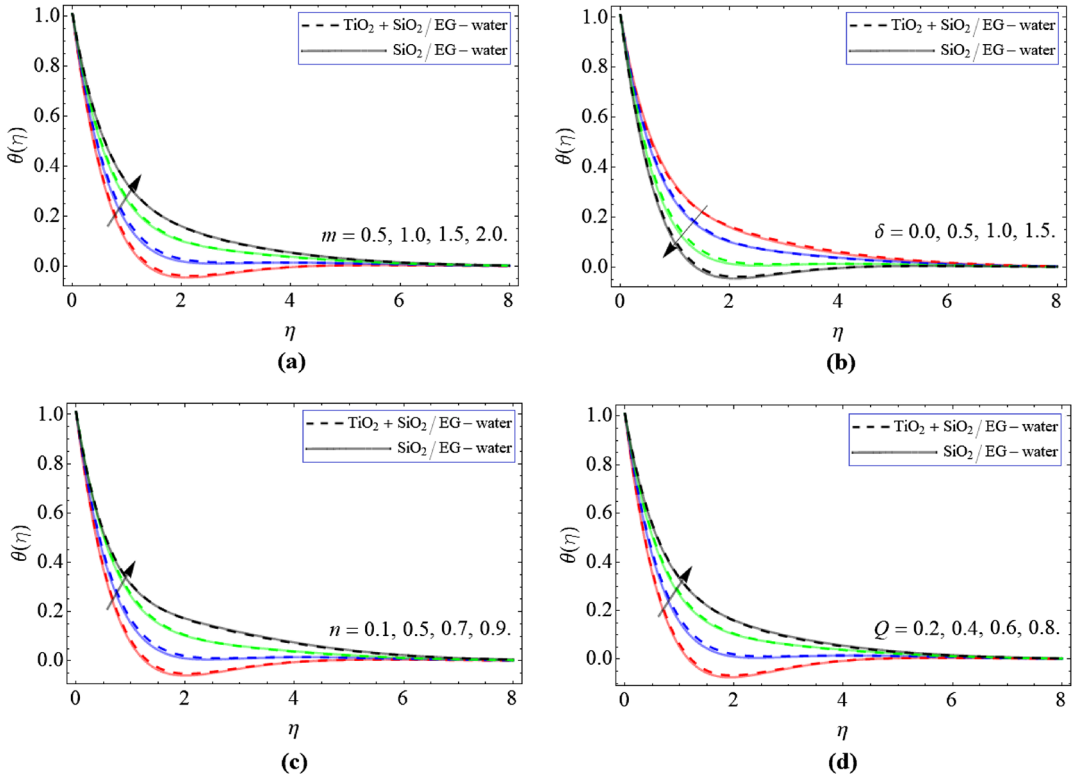

Figure 4. The exposition of energy $\theta(\eta)$ curve versus the m, δ, n and Q respectively.

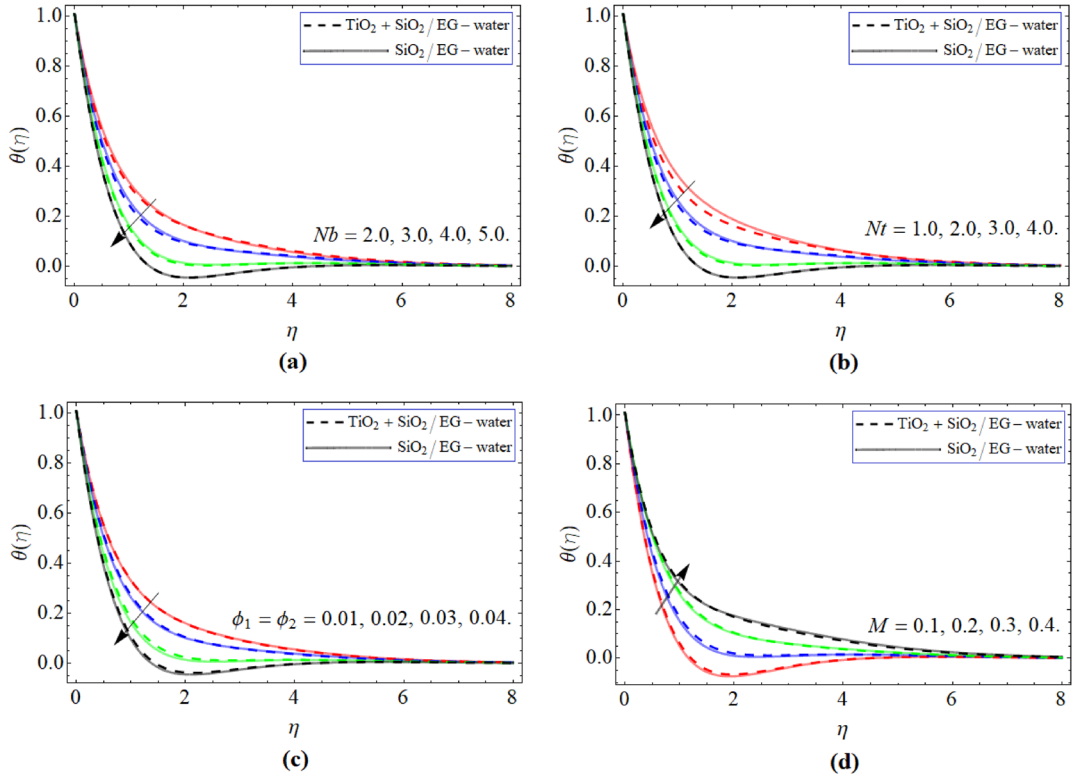

Figure 5. The exposition of energy $\theta(\eta)$ curve verus the Nb, Nt, ϕ_1, ϕ_2 and M respectively.

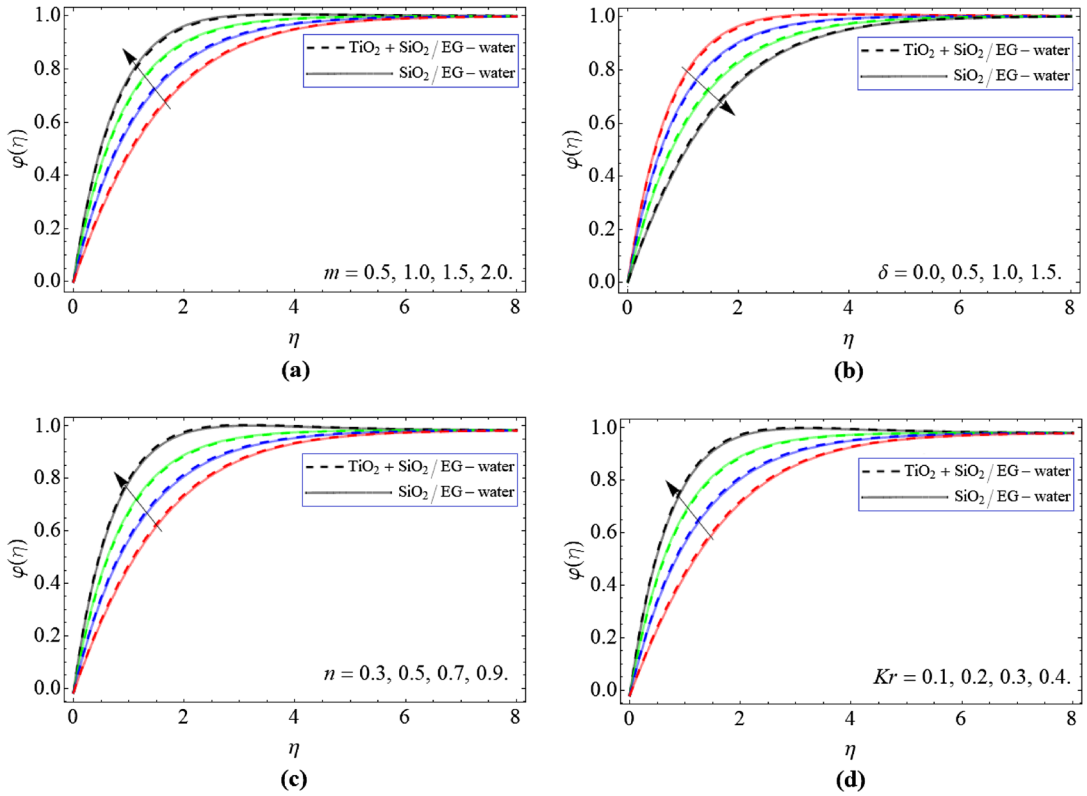

Figure 6. The concentration $\varphi(\eta)$ outline versus m, δ, n and Kr respectively.

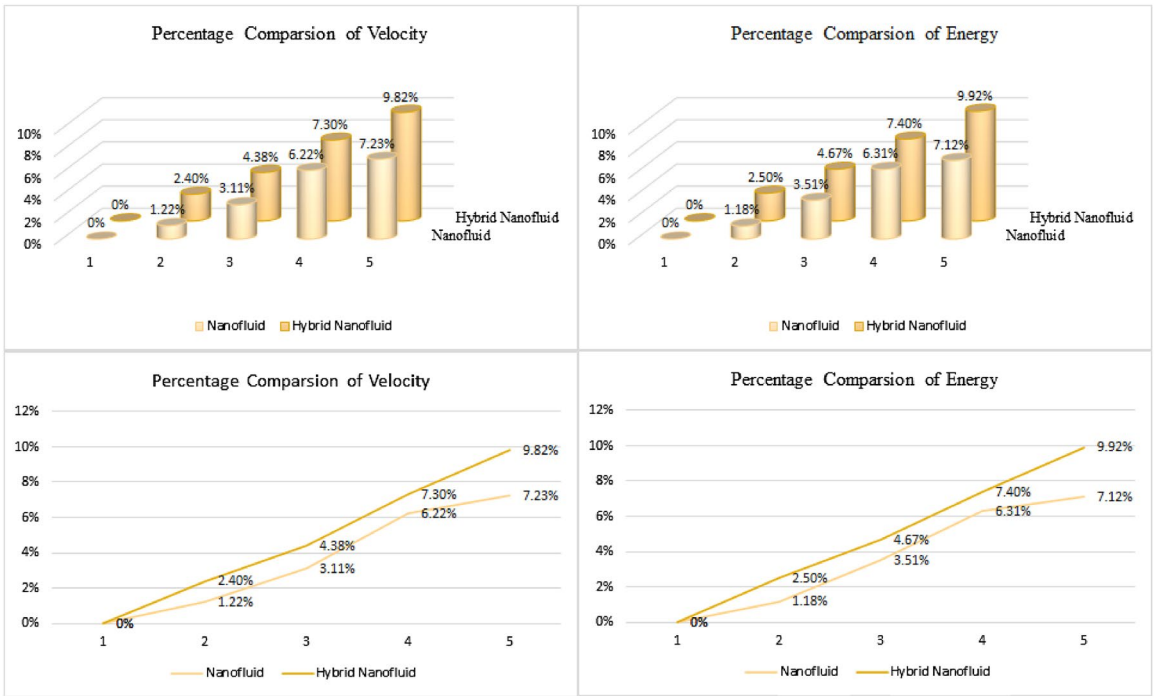

Figure 7. The comparation between nanoliquid and hybrid nanoliquid.

Nano particulates and base fluid	$\rho\ (kg/m^3)$	$k\ (W/mK)$	$Cp\ (j/kg\ K)$	$\sigma\ (S/m)$
$C_2H_6O_2$–H_2O	1063.8	0.387	3630	0.00509
SiO_2	2270	1.4013	3630	3.5×10^6
TiO_2	4250	8.953	686.2	2.38×10^6

Table 1. The tentative values of TiO_2, TiO_2 and $C_2H_6O_2$–H_2O[44].

Models
$\frac{\mu_{hnf}}{\mu_{bf}} = \frac{1}{(1-\phi_{SiO_2}-\phi_{TiO_2})^2}$
$\frac{\rho_{hnf}}{\rho_{bf}} = \phi_{SiO_2}\left(\frac{\rho_{SiO_2}}{\rho_{bf}}\right) + \phi_{TiO_2}\left(\frac{\rho_{TiO_2}}{\rho_{bf}}\right) + \left(1-\phi_{SiO_2}-\phi_{TiO_2}\right)$
$\frac{(\rho C_p)_{hnf}}{(\rho C_p)_{bf}} = \phi_{SiO_2}\left(\frac{(\rho C_p)_{SiO_2}}{(\rho C_p)_{bf}}\right) + \phi_{TiO_2}\left(\frac{(\rho C_p)_{TiO_2}}{(\rho C_p)_{bf}}\right) + \left(1-\phi_{SiO_2}-\phi_{TiO_2}\right)$
$\frac{(\rho\beta_T)_{hnf}}{(\rho\beta_T)_{bf}} = \phi_{SiO_2}\left(\frac{(\rho\beta_T)_{SiO_2}}{(\rho\beta_T)_{bf}}\right) + \phi_{TiO_2}\left(\frac{(\rho\beta_T)_{TiO_2}}{(\rho\beta_T)_{bf}}\right) + \left(1-\phi_{SiO_2}-\phi_{TiO_2}\right)$
$\frac{k_{hnf}}{k_{bf}} = \left[\frac{\left(\frac{\phi_{SiO_2}k_{SiO_2}+\phi_{TiO_2}k_{TiO_2}}{\phi_{SiO_2}+\phi_{TiO_2}}\right)+2k_{bf}+2\left(\phi_{SiO_2}k_{SiO_2}+\phi_{TiO_2}k_{TiO_2}\right)-2\left(\phi_{SiO_2}+\phi_{TiO_2}\right)k_{bf}}{\left(\frac{\phi_{SiO_2}k_{SiO_2}+\phi_{TiO_2}k_{TiO_2}}{\phi_{SiO_2}+\phi_{TiO_2}}\right)+2k_{bf}-2\left(k_{SiO_2}\phi_{SiO_2}+k_{TiO_2}\phi_{TiO_2}\right)+2\left(\phi_{SiO_2}+\phi_{TiO_2}\right)k_{bf}}\right]$
$\frac{\sigma_{hnf}}{\sigma_{bf}} = \left[\frac{\left(\frac{\sigma_{SiO_2}\phi_{SiO_2}+\phi_{TiO_2}\sigma_{TiO_2}}{\phi_{TiO_2}+\phi_{SiO_2}}\right)+2\sigma_{bf}+2\left(\sigma_{SiO_2}\phi_{SiO_2}+\phi_{TiO_2}\sigma_{TiO_2}\right)-2\left(\phi_{SiO_2}+\phi_{TiO_2}\right)\sigma_{bf}}{\left(\frac{\phi_{SiO_2}\sigma_{SiO_2}+\phi_{TiO_2}\sigma_{TiO_2}}{\phi_{SiO_2}+\phi_{TiO_2}}\right)+2\sigma_{bf}-\left(\sigma_{SiO_2}\phi_{SiO_2}+\phi_{TiO_2}\sigma_{TiO_2}\right)+\left(\phi_{SiO_2}+\phi_{TiO_2}\right)\sigma_{bf}}\right]$

Table 2. The mathematical model of the hybrid nanoliquid $\left(\phi_1 = \phi_{SiO_2},\ \phi_2 = \phi_{TiO_2}\right)$[44].

			bvp4c	ND-solve
n	Ref.[41] $-f''(0)$	Ref.[45] $-f''(0)$	Current outcomes $-f''(0)$	Current outcomes $-f''(0)$
1.0	1.000001	1.0000	1.000000	1.000000
2.0	1.023410	1.0234	1.023511	1.023500
3.0	1.035871	1.0359	1.035970	1.035961
5.0	1.048615	1.0486	1.048514	1.048503
7.0	1.055049	1.0550	1.055248	1.055227
9.0	1.058920	1.0589	1.058941	1.058901
10	1.060329	1.0603	1.060428	1.060407

Table 3. The numerical outcomes for skin friction $-f''(0)$.

m	δ	N	C_{f_x}	C_{f_z}	Nu_r	Sh_r
0.2			−1.689775	0.418367	1.225167	3.371834
0.4			−1.286627	0.685572	1.259011	3.234460
0.6			−1.865864	0.726487	1.289550	3.104671
0.8			−0.1646348	0.765092	1.412453	3.006296
1.0			−1.496956	0.791047	1.429020	2.935582
	0.1		−1.509798	0.420456	1.18262	1.723911
	0.2		−1.689775	0.418367	1.625167	2.371834
	0.3		−1.877942	0.414772	1.701782	6.058711
	0.4		−1.074212	0.409747	2.303375	8.311254
	0.5		−1.278457	0.403394	2.723852	10.47904
		0.2	−1.689775	0.418367	1.325167	5.371834
		0.3	−2.214652	0.497395	1.253300	3.381260
		0.4	−2.686005	0.567704	1.265827	2.474134
		0.5	−3.116150	0.631884	1.222736	0.677470
		0.6	−3.513876	0.691371	1.206127	0.572587

Table 4. The numerical results for $\left(C_{f_x},\ C_{f_z}\right)$,$Nu_r$ and Sh_r.

Data availability

All data used in this manuscript have been presented within the article.

Received: 31 July 2022; Accepted: 15 September 2022
Published online: 29 September 2022

References

1. Mjankwi, M. A., Masanja, V. G., Mureithi, E. W., & James, M. N. O. (2019). Unsteady MHD flow of nanofluid with variable properties over a stretching sheet in the presence of thermal radiation and chemical reaction. *Int. J. Math. Math. Sci*. (2019).
2. Varun Kumar, R. S., Punith Gowda, R. J., Naveen Kumar, R., Radhika, M. & Prasannakumara, B. C. Two-phase flow of dusty fluid with suspended hybrid nanoparticles over a stretching cylinder with modified Fourier heat flux. *SN Appl. Sci.* **3**(3), 1–9 (2021).
3. Varun Kumar, R. S., Alhadhrami, A., Punith Gowda, R. J., Naveen Kumar, R. & Prasannakumara, B. C. Exploration of Arrhenius activation energy on hybrid nanofluid flow over a curved stretchable surface. *ZAMM-J. Appl. Math. Mech./Zeitschrift für Angewandte Mathematik und Mechanik* **101**(12), e202100035 (2021).
4. Gul, T. *et al.* Magnetic dipole impact on the hybrid nanofluid flow over an extending surface. *Sci. Rep.* **10**(1), 1–13 (2020).
5. Bilal, M. *et al.* Comparative numerical analysis of Maxwell's time-dependent thermo-diffusive flow through a stretching cylinder. *Case Stud. Thermal Eng.* **27**, 101301 (2021).
6. SafwaKhashiie, N., MdArifin, N., Hafidzuddin, E. H. & Wahi, N. Dual stratified nanofluid flow past a permeable shrinking/stretching sheet using a non-Fourier energy model. *Appl. Sci.* **9**(10), 2124 (2019).
7. Hussain, A. *et al.* Three-dimensional water-based magneto-hydrodynamic rotating nanofluid flow over a linear extending sheet and heat transport analysis: A numerical approach. *Energies* **14**(16), 5133 (2021).
8. Shuaib, M., Bilal, M., Khan, M. A. & Malebary, S. J. Fractional analysis of viscous fluid flow with heat and mass transfer over a flexible rotating disk. *Comput. Model. Eng. Sci.* **123**(1), 377–400 (2020).
9. Hussain, A. *et al.* Heat transfer and flow characteristics of pseudoplastic nanomaterial liquid flowing over the slender cylinder with variable characteristics. *Curr. Comput.-Aided Drug Des.* **12**(1), 27 (2022).
10. Uddin, Z., Vishwak, K. S. & Harmand, S. Numerical duality of MHD stagnation point flow and heat transfer of nanofluid past a shrinking/stretching sheet: Metaheuristic approach. *Chin. J. Phys.* **73**, 442–461 (2021).
11. Rasool, G. *et al.* Numerical scrutinization of Darcy–Forchheimer relation in convective magnetohydrodynamic nanofluid flow bounded by nonlinear stretching surface in the perspective of heat and mass transfer. *Micromachines* **12**(4), 374 (2021).
12. Ahmad, S. *et al.* Impact of Joule heating and multiple slips on a Maxwell nanofluid flow past a slendering surface. *Commun. Theor. Phys.* **74**(1), 015001 (2021).
13. Ahmadian, A., Bilal, M., Khan, M. A. & Asjad, M. I. The non-Newtonian maxwell nanofluid flow between two parallel rotating disks under the effects of magnetic field. *Sci. Rep.* **10**(1), 1–14 (2020).
14. Song, Y. Q. *et al.* Physical impact of thermo-diffusion and diffusion-thermo on Marangoni convective flow of hybrid nanofluid ($MnZiFe_2O_4$–$NiZnFe_2O_4$–H_2O) with nonlinear heat source/sink and radiative heat flux. *Mod. Phys. Lett. B* **35**(22), 2141006 (2021).
15. Khan, M. I. *et al.* Marangoni convective flow of hybrid nanofluid ($MnZnFe_2O_4$–$NiZnFe_2O_4$–H_2O) with Darcy Forchheimer medium. *Ain Shams Eng. J.* **12**(4), 3931–3938 (2021).
16. Li, Y. X. *et al.* Dynamics of aluminum oxide and copper hybrid nanofluid in nonlinear mixed Marangoni convective flow with entropy generation: Applications to renewable energy. *Chin. J. Phys.* **73**, 275–287 (2021).
17. Kazemi, M., Ghobadi, M. & Mirzaie, A. Cobalt ferrite nanoparticles ($CoFe_2O_4$ MNPs) as catalyst and support: magnetically recoverable nanocatalysts in organic synthesis. *Nanotechnol. Rev.* **7**(1), 43–68 (2018).
18. Traciak, J., Sobczak, J., Kuzioła, R., Wasąg, J. & Żyła, G. Surface and optical properties of ethylene glycol-based nanofluids containing silicon dioxide nanoparticles: An experimental study. *J. Therm. Anal. Calorim.* **147**(14), 7665–7673 (2022).
19. Bhatti, M. M., Öztop, H. F., Ellahi, R., Sarris, I. E. & Doranehgard, M. H. Insight into the investigation of diamond (C) and Silica (SiO_2) nanoparticles suspended in water-based hybrid nanofluid with application in solar collector. *J. Mol. Liq.* **357**, 119134 (2022).
20. Ahmed, J. *et al.* Thermal analysis in swirling flow of titanium dioxide–aluminum oxide water hybrid nanofluid over a rotating cylinder. *J. Therm. Anal. Calorim.* **144**(6), 2175–2185 (2021).
21. Khashi'ie, N. S., Md Arifin, N., Pop, I., & Nazar, R. (2020). Melting heat transfer in hybrid nanofluid flow along a moving surface. *J. Thermal Anal. Calorim.* **147**, 567–578 (2022).
22. Khashi'ie, N. S., Waini, I., Zokri, S. M., Kasim, A. R. M., Arifin, N. M., & Pop, I. (2021). Stagnation point flow of a second-grade hybrid nanofluid induced by a Riga plate. *Int. J. Numer. Methods Heat Fluid Flow*.
23. Alwawi, F., Sulaiman, I. M., Swalmeh, M. Z., & Yaseen, N. (2022). Energy transport boosters of magneto micropolar fluid flowing past a cylinder: A case of laminar combined convection. in *Proceedings of the Institution of Mechanical Engineers, Part C: Journal of Mechanical Engineering Science*, 09544062221111055.
24. Abbasi, A., Gul, M., Farooq, W., Khan, S. U., Aydi, A., Ayadi, B., *et al.* (2022). A comparative thermal investigation for modified hybrid nanofluid model (Al_2O_3–SiO_2–TiO_2)/($C2H_6O_2$) due curved radiated surface. *Case Stud. Thermal Eng*. 102295.
25. Khashi'ie, N. S., Waini, I., Ishak, A. & Pop, I. Blasius flow over a permeable moving flat plate containing Cu–Al_2O_3 hybrid nanoparticles with viscous dissipation and radiative heat transfer. *Mathematics* **10**(8), 1281 (2022).
26. De, P. Soret-Dufour effects on unsteady flow of convective Eyring-Powell magneto nanofluids over a semi-infinite vertical plate. *BioNanoScience* **9**(1), 7–12 (2019).
27. Mondal, H., De, P., Goqo, S., & Sibanda, P. (2020). A numerical study of nanofluid flow over a porous vertical plate with internal heat generation and nonlinear thermal radiation. *J. Porous Media*. **23**(6).
28. Khan, U., Ahmed, N., Mohyud-Din, S. T., Alsulami, M. D. & Khan, I. A novel analysis of heat transfer in the nanofluid composed by nanodimaond and silver nanomaterials: numerical investigation. *Sci. Rep.*, **12**(1), 1–11 (2022).
29. Xiong, P. Y. *et al.* Comparative analysis of (Zinc ferrite, Nickel Zinc ferrite) hybrid nanofluids slip flow with entropy generation. *Mod. Phys. Lett. B* **35**(20), 2150342 (2021).
30. Kumar, R. N. *et al.* Impact of magnetic dipole on ferromagnetic hybrid nanofluid flow over a stretching cylinder. *Phys. Scr.* **96**(4), 045215 (2021).
31. Hamid, A., Naveen Kumar, R., Punith Gowda, R. J., Varun Kumar, R. S., Khan, S. U., Ijaz Khan, M., *et al.* Impact of Hall current and homogenous–heterogenous reactions on MHD flow of GO-MoS2/water (H2O)-ethylene glycol (C2H6O2) hybrid nanofluid past a vertical stretching surface. *Waves Random Complex Media*. https://doi.org/10.1080/17455030.2021.1985746 (2021).
32. Punith Gowda, R. J., Naveen Kumar, R., Jyothi, A. M., Prasannakumara, B. C. & Sarris, I. E. Impact of binary chemical reaction and activation energy on heat and mass transfer of marangoni driven boundary layer flow of a non-Newtonian nanofluid. *Processes* **9**(4), 702 (2021).
33. De, P. & Gorji, M. R. Activation energy and binary chemical reaction on unsteady MHD Williamson nanofluid containing motile gyrotactic micro-organisms. *Heat Transfer* **49**(5), 3030–3043 (2020).
34. Sangeetha, E., & De, P. (2021). Bioconvection in nanofluid flow embedded in non-Darcy porous medium with viscous dissipation and Ohmic heating. *J. Porous Media*. **24**(1).

35. Khan, M. N. & Nadeem, S. A comparative study between linear and exponential stretching sheet with double stratification of a rotating Maxwell nanofluid flow. *Surfaces Interfaces* **22**, 100886 (2021).
36. Acharya, N., Mabood, F., Shahzad, S. A. & Badruddin, I. A. Hydrothermal variations of radiative nanofluid flow by the influence of nanoparticles diameter and nanolayer. *Int. Commun. Heat Mass Transfer* **130**, 105781 (2022).
37. Khashi'ie, N. S., Arifin, N. M. & Pop, I. Magnetohydrodynamics (MHD) boundary layer flow of hybrid nanofluid over a moving plate with Joule heating. *Alex. Eng. J.* **61**(3), 1938–1945 (2022).
38. Waini, I. *et al.* Unsteady magnetohydrodynamics (MHD) flow of hybrid ferrofluid due to a rotating disk. *Mathematics* **10**(10), 1658 (2022).
39. Gouran, S., Mohsenian, S. & Ghasemi, S. E. Theoretical analysis on MHD nanofluid flow between two concentric cylinders using efficient computational techniques. *Alex. Eng. J.* **61**(4), 3237–3248 (2022).
40. Shamshuddin, M. D., & Ibrahim, W. Finite element numerical technique for magneto-micropolar nanofluid flow filled with chemically reactive casson fluid between parallel plates subjected to rotatory system with electrical and Hall currents. *Int. J. Model. Simulat*. https://doi.org/10.1080/02286203.2021.2012634 (2022).
41. Das, K., Giri, S. S. & Kundu, P. K. Influence of Hall current effect on hybrid nanofluid flow over a slender stretching sheet with zero nanoparticle flux. *Heat Transfer* **50**(7), 7232–7250 (2021).
42. Shuaib, M., Shah, R. A., Durrani, I. & Bilal, M. Electrokinetic viscous rotating disk flow of Poisson-Nernst-Planck equation for ion transport. *J. Mol. Liq.* **313**, 113412 (2020).
43. Shuaib, M., Shah, R. A. & Bilal, M. Von-Karman rotating flow in variable magnetic field with variable physical properties. *Adv. Mech. Eng.* **13**(2), 1687814021990463 (2021).
44. Haq, I., Bilal, M., Ahammad, N. A., Ghoneim, M. E., Ali, A., & Weera, W. (2022). Mixed convection nanofluid flow with heat source and chemical reaction over an inclined irregular surface. *ACS Omega*.
45. Khader, M. M. & Megahed, A. M. Boundary layer flow due to a stretching sheet with a variable thickness and slip velocity. *J. Appl. Mech. Tech. Phys.* **56**(2), 241–247 (2015).

Acknowledgements

The author (Z. Raizah) extends her appreciation to the Deanship of Scientific Research at King Khalid University, Abha, Saudi Arabia, for funding this work through the Research Group Project under Grant number (RGP.1/334/43).

Author contributions

All authors equally contributed.

Competing interests

The authors declare no competing interests.

Additional information

Correspondence and requests for materials should be addressed to P.J.

Reprints and permissions information is available at www.nature.com/reprints.

Publisher's note Springer Nature remains neutral with regard to jurisdictional claims in published maps and institutional affiliations.